Richter et al., http://www.jcb.org/cgi/content/full/jcb.201311014/DC1

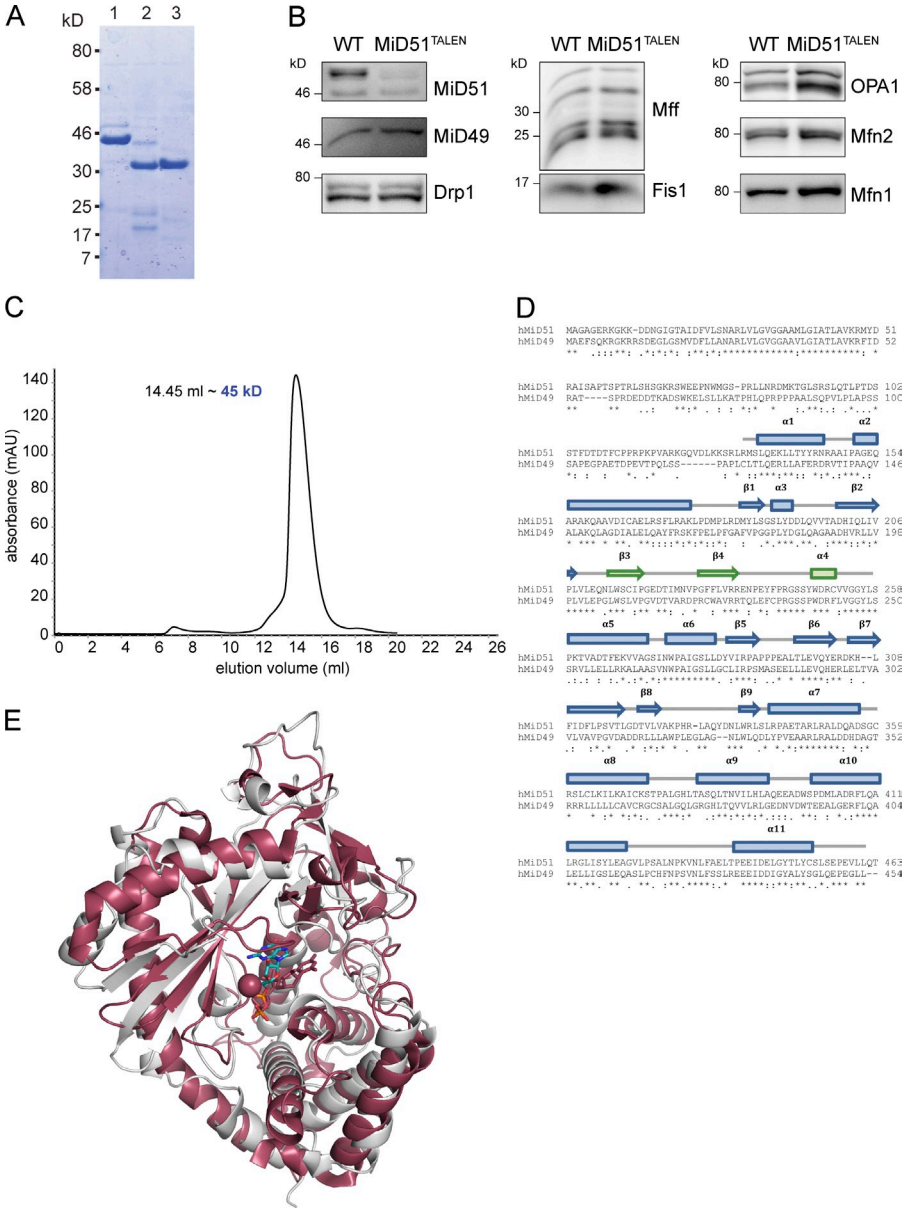

Figure S1. **Recombinant protein expression, TALEN knockout, and structural characterization of MiD51.** (A) Limited proteolysis of mouse MiD49$^{\Delta N50}$ (1) using chymotrypsin (2) and trypsin (3). (B) Western blot analysis of mitochondrial dynamics proteins in wild -type MEFs and MEF clonal cell line lacking MiD51 (MiD51^{TALEN}). (C) Gel filtration chromatogram of MiD51$^{\Delta N118}$ eluting as a single peak, corresponding to a 45-kD species according to a standard curve. (D) Sequence alignment of MiD51 and MiD49. Sequence numbers and secondary structure elements are included above the alignment and colored as in Fig. 1 B. (E) Superimposition of wild-type MiD51 (gray) with cGAS (PDB accession no. 4JLZ; burgundy).

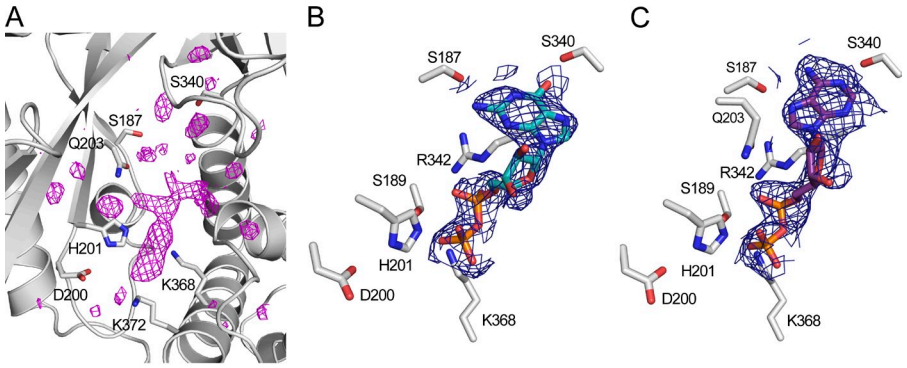

D

	Non-nucleotide bound MiD51	MiD51-ADP	MiD51-GDP	MiD51$^{\Delta PEYFP}$-ADP	MiD51$^{\Delta PEYFP}$-GDP
Non-nucleotide bound MiD51	0	0.56 (328)	0.63 (330)	1.12 (313)	1.12 (312)
MiD51-ADP	0.56 (328)	0	0.37 (327)	1.14 (310)	1.17 (310)
MiD51-GDP	0.63 (330)	0.37 (327)	0	1.32 (315)	1.27 (312)
MiD51$^{\Delta PEYFP}$-ADP	1.12 (313)	1.14 (310)	1.32 (315)	0	0.18 (325)
MiD51$^{\Delta PEYFP}$-GDP	1.12 (312)	1.17 (310)	1.27 (312)	0.18 (325)	0

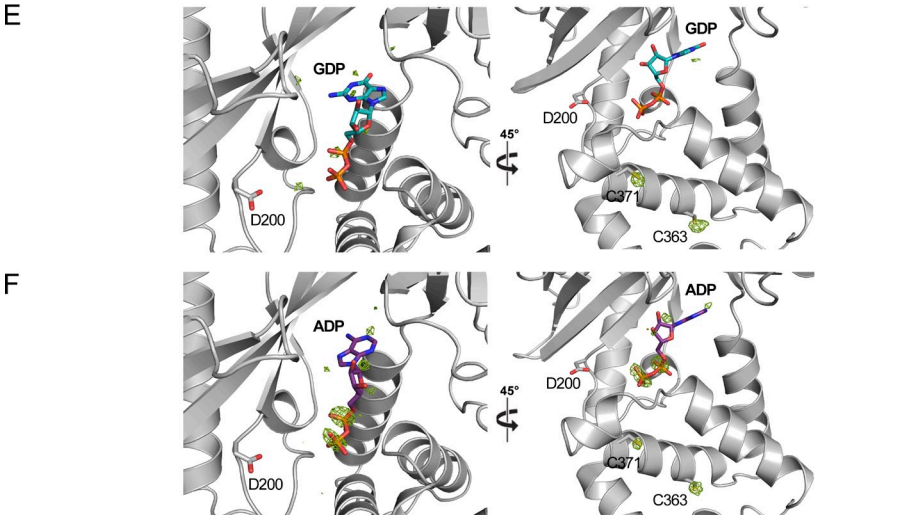

Figure S2. **Structural characterization of the MiD51 nucleotide binding pocket.** (A) Difference (F_oF_{cwt}) map displayed around the nucleotide binding pocket of native MiD51 showing additional unidentified density. Map was rendered in Pymol, contoured at 3.0 δ, and carved at 5.0 Å. (B and C) Simulated anneal omit maps (dark blue) calculated in PHENIX for GDP (B) and ADP (C) molecules, contoured at 1 δ. (D) RMSDs between monomers of all crystallized forms of MiD51 and MiD51$^{\Delta PEYFP}$. For structures containing four monomers in the asymmetric unit, the monomer lacking the fewest atoms was used for alignments. Aligned α-carbons are indicated in parentheses. (E and F) Anomalous difference map (green) of nucleotide binding pocket in GDP-MiD51 (E) and ADP-MiD51 (F) generated in FFT and contoured at 3.0 δ. Anomalous signal for two sulfurs on C363 and C371 is shown in 45° rotations, as well as for the two phosphates in ADP.

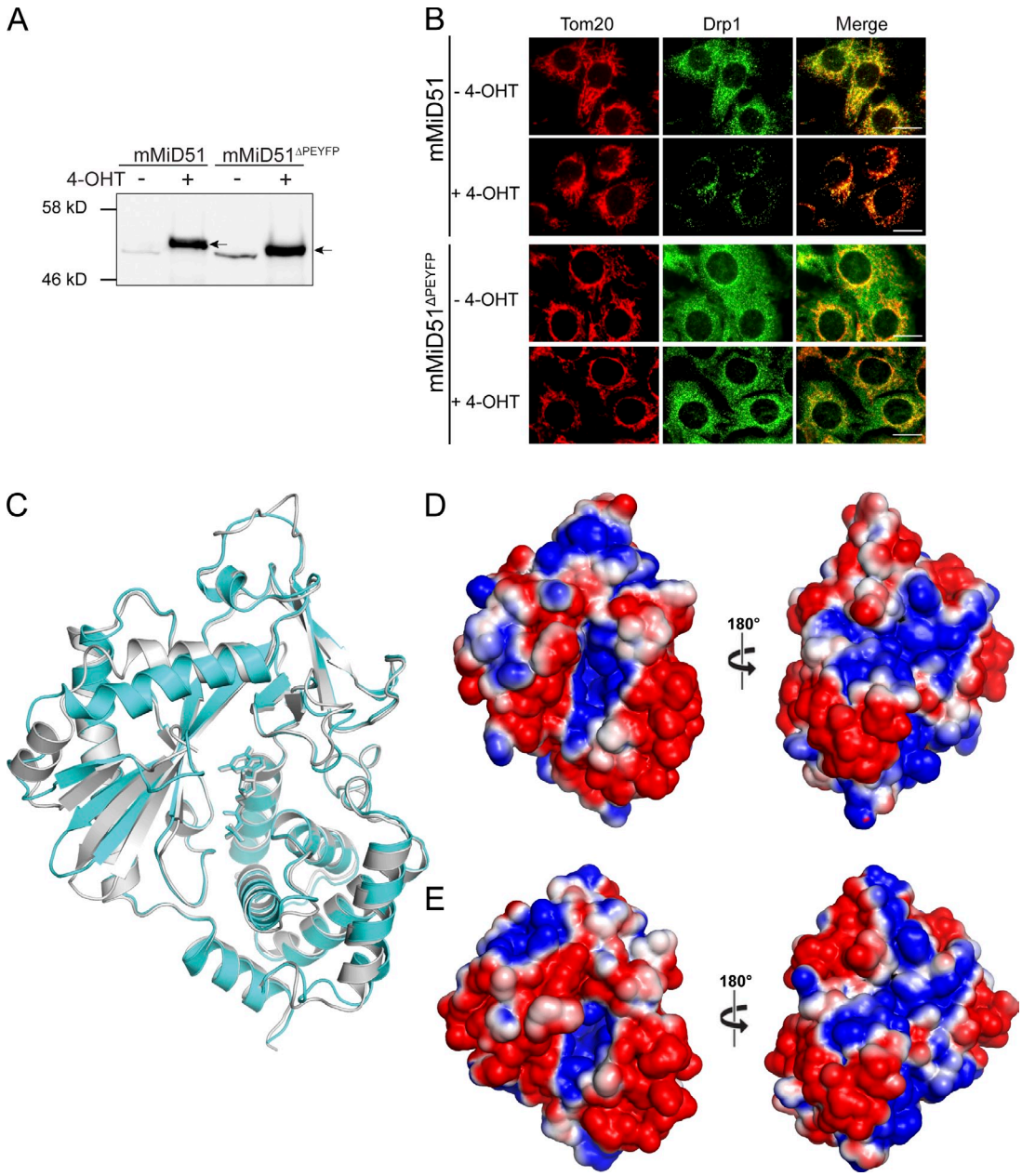

Figure S3. **Structural and functional analysis of the MiD51$^{\Delta PEYFP}$ mutant.** 4-OHT–induced expression of wild-type mouse MiD51 or MiD51$^{\Delta PEYFP}$ in lentiviral-transduced MiD51^{TALEN} cells lacking endogenous MiD51 was analyzed by immunoblotting (A) and cells were immunostained for the mitochondrial marker protein Tom20 (red) and Drp1 (green; B). Bars, 20 µm. (C) SSM superposition of GDP-MiD51$^{\Delta N118}$ (gray) and GDP-MiD51$^{\Delta N118/PEYFP}$ (cyan) crystal structures. (D) Electrostatic surface potential of MiD51$^{\Delta N118}$. (E) Electrostatic surface potential of MiD51$^{\Delta N118/PEYFP}$.

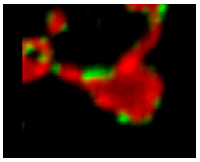

Video 1. **Time-lapse imaging showing a fission event at MiD51-GFP foci in a COS-7 cell.** COS-7 cells were transfected with MiD51-GFP (green) and stained for mitochondria with MitoTracker deep red (red). Time-lapse image analysis was performed using a laser-scanning confocal microscope (LSM 510; Carl Zeiss) equipped with a ConfoCor 3 system containing an avalanche photodiode detector using a 40× oil objective. Images were recorded every 5.5 s.

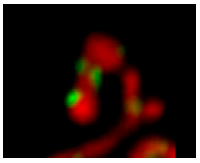

Video 2. **Time-lapse imaging showing a fission event at MiD51-GFP foci in a COS-7 cell.** COS-7 cells were transfected with MiD51-GFP (green) and stained for mitochondria with MitoTracker deep red (red). Time-lapse image analysis was performed using a laser-scanning confocal microscope (LSM 510; Carl Zeiss) equipped with a ConfoCor 3 system containing an avalanche photodiode detector using a 40× oil objective. Images were recorded every 5.5 s.

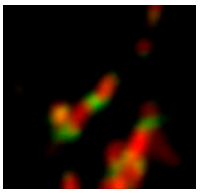

Video 3. **Fission events occur at MiD51^{NBD}-GFP foci.** MiD51^{TALEN} MEFs were induced for 4 h with 100 nM 4-OHT to express MiD51-GFP or MiD51^{NBD}-GFP (green). Cells were stained for mitochondria with MitoTracker red (red). A composite of three separate fission events in different cells is shown. Time-lapse image analysis was performed using a laser-scanning confocal microscope (LSM 510; Carl Zeiss) equipped with a ConfoCor 3 system containing an avalanche photodiode detector using a 40× oil objective. Images were recorded every 5.5 s.